Supporting information for

Sacrificial ZIF-L Seed Layer for Sub-100 nm Thin Propylene-Selective ZIF-8 Membranes

*Chanjong Yu[a], Yeong jae Kim[a], Jongbum Kim[a], Mikio Hayashi[b], Dae Woo Kim[c], Hyuktaek Kwon[*d], Kiwon Eum[*a]*

*Corresponding author: htkwon@pknu.ac.kr, and kiwon.eum@ssu.ac.kr

[a]School of Chemical Engineering, Soongsil University, Seoul, 06978 Republic of Korea

[b]Science & Innovation Center, Mitsubishi Chemical Corporation, 1000 Kamoshida-cho, Aoba-ku, Yokohama-shi, Kanagawa 227-8502, Japan

[c]Department of Chemical and Biomolecular Engineering, Yonsei University, Yonsei-ro 50, Seodaemun-gu, Seoul 03722, Republic of Korea

[d]School of Chemical Engineering, Pukyong National University, 45 Yongso-ro, Nam-gu, Busan, 48513 Republic of Korea

Materials 2-methylimidazole (99%, 2mIm), zinc acetate dihydrate (99%, $Zn(OAc)_2 \cdot 2H_2O$), zinc nitrate hexahydrate (98%, $Zn(NO_3)_2 \cdot 6H_2O$), Nitric acid (70%, HNO_3) and 1-Octanol (≥99%, $C_8H_{18}O$) were obtained from Sigma-Aldrich. Ethyl alcohol anhydrate (99.9%, C_2H_5OH) and N,N-Dimethylacetamide (99.5%, DMAc) were purchased from DaeJong-Chem. Alumina powder (CR6, α-Al_2O_3) was obtained from Baikowski. Deionized water (DI-water) was produced by Direct-Pure Up (Rephile Bioscience).

ZIF-L crystals synthesis 0.28 g $Zn(NO_3)_2 \cdot 6H_2O$ was dissolved in 7 ml DI-water and 0.77 g 2mIm was dissolved in 14 ml DI-water, respectively. Then, 14 ml of 2mIm aqueous solution was added dropwise to zinc nitrate aqueous solution while stirring. Finally, the cloudy solution was sustained stationary for 8 h at room temperature and was centrifuged at 11000 rpm for 40 min. As-made ZIF-L powders were washed with DI-water three times and then dried in a vacuum oven at 80 ˚C for 12 h.

ZIF-8 nanocrystals synthesis ZIF-8 nanocrystals were synthesized reported by Lai *et al*. [1] 1.17 g $Zn(NO_3)_2 \cdot 6H_2O$ was dissolved in 8 ml DI-water and 22.7 g 2mIm was dissolved in 80 ml DI-water, respectively. While stirring the 2mIm aqueous solution slowly poured into the zinc nitrate aqueous solution. The solution was stirred for 5 min at room temperature and was centrifuged at 11000 rpm for 40 min. The resulting powder was washed with DI- water at three times and then dried in a vacuum oven at 80 ˚C for 12 h.

Transformation from ZIF-L to ZIF-8 crystals 0.26 g $Zn(OAc)_2 \cdot 2H_2O$ and 0.2 g 2mIm was dissolved in 3 ml of DMAc/H_2O (2:1 v/v) solution, respectively. The solution was segmented overnight, and only top transparent part of the solution was collected. Then, 0.03 g of ZIF-L crystal was putted into the Petri dish and prepared solution was dropped on the ZIF-L crystal to soak

thoroughly. Then, Petri dish was placed in an oven preheated to 473 K for 15 min and cool down naturally. Crystals were washed with DI-water three times followed by vacuum degassing at 80 ˚C overnight. For solvent effect investigation, DMAc/H_2O (2:1 v/v) solution was prepared without adding any organic and inorganic precursors. Then, 0.08 g ZIF-L crystal was dissolved in 8 mL DMAc/H_2O (2:1 v/v) solution by sonication. The vial was placed in an oven preheated to 333 K at different time points (0.5 h, 1 h, 2 h, 4 h and 8 h) and allowed to cool naturally. The solution was centrifuged at 11000 rpm for 40 min. The resulting powder was washed with DI-water at three times and then dried in a vacuum oven at 80 ˚C for 12 h.

Preparation of α-alumina support α-alumina supports (diameter : 22 mm) with an average pore diameter of 200 nm were fabricated as previously reported [2]. Briefly, 22 g of alumina powder (CR6, Baikowski) and 228 μL of 1M Nitric acid was homogeneously mixed with 22 g of DI-water. Upon mixing, the solution was horn sonicated for several minutes followed by degassing for uniform dispersion of the alumina particles. Then, approximately 2.9 mL of alumina suspension was transferred to a PTFE cylinder holder fitted with a nylon filter paper (0.2 μm, Whatman) and a weak vacuum (~14 kPa) was applied to remove excess water from the alumina suspension for proper molding. The vacuum was released after 1 h, and the obtained alumina disk was dried overnight. As-formed alumina disk was then sintered at 1323 K with a ramping rate of 2 K/min. Then one side of the sintered disks was polished using a sandpaper (grid #1400) to reduce the surface roughness of the supports, followed by sonication for 1 min in Ethanol. Subsequently the supports were dried in an oven at 200 ˚C for 0.5 h before usage.

Preparation of the hetero-epitaxially grown ZIF-L seeded ZIF-8 membrane Case 1 ZIF-8 membrane was fabricated by modifying the procedure reported by Jeong *et al*. [3] 0.26 g $Zn(OAc)_2$

· $2H_2O$ and 0.2 g 2mIm was dissolved in 3 ml of DMAc/DI-water (2:1 v/v) solution respectively. The ligand solution was added dropwise while stirring the metal salt solution and stirred to form a cloudy solution. The transparent part was obtained by allowing the solution to settle for overnight. Prepared transparent ZIF-8 growth solution was gently poured into petri dish and α-alumina support was coated for 10 s. Then, coated support was placed in an oven preheated to 473 K for 15 min and allowed to cool naturally. For Case 2 and Case 3 membranes, ZIF-8 (Case 2) or ZIF-L (Case 3) seed layered α-alumina support was used. Other procedure was identical as Case 1. For seed layer preparation, approximately 0.01 g of powders were gently rubbed on the surface of a α-alumina support followed by soaked in EtOH for 10 s.

Characterization X-ray diffraction patterns were obtained from Bruker D2 Phaser diffractometer at ambient temperature using Cu Kα radiation of λ = 0.154 nm and a scanning range of 5−40° 2θ. Nanocrystals and membrane SEM images were collected with ZEISS GeminiSEM 300. All membrane samples were pretreated with sputter coated with Pt (Q150R Plus-Rotary Pumped Coater). N_2 physisorption isotherms were obtained from a Micromeritics ASAP 2020 surface area analyzer at 77 K.

Gas permeation test C_3H_6/C_3H_8 binary gas permeation measurements were carried out at by the Wicke−Kallenbach (W-K) technique, as shown in **Figure S10**. Briefly, equimolar C_3H_6/C_3H_8 binary mixture was used as feed side. Argon was used as sweep gas for the permeate stream. The C_3H_6/C_3H_8 mixture and argon gases were supplied to the feed and permeate sides at a flow rate of 20 SCCM, respectively. The feed pressure can be controlled by back-pressure controller range by 1~4 bar. The membrane temperature can be controlled by forced convection oven (Yamato DKN312C). The composition of the permeate side stream was analyzed using online gas

chromatography (Agilent GC 6890N). At each measurement, the system was stabilized for at least 4 h and the measurement was repeated several times until reaches steady state value.

The permeance of gas through the membrane, F_i, is defined as:

$$F_i = \frac{R_i}{A \cdot \Delta P_i}$$

Where, R_i is the mole rate of component *i* (mol/s), ΔP_i is the partial pressure difference component *i* (Pa) across the membrane, and A is the effective membrane area (m^2).

The permeability of gas through the membrane, P_i, is defined as:

$$P_i = F_i \cdot l$$

Where, l is the thickness of membrane (m).

The Selectivity ($\alpha_{i,j}$) for component *i* over component *j* is defined as:

$$\alpha_{i,j} = \frac{P_i}{P_j}$$

Where, P_i and P_j are the permeability of components i and j ($\frac{mol \cdot m}{m^2 \cdot Pa \cdot s}$).

The Separation factor ($\alpha_{i,j}$) for component *i* over component *j* is defined as:

$$\alpha_{i,j} = \frac{y_i / y_j}{x_i / x_j}$$

Where, x_i and x_j are the molar fraction of components i and j in the feed stream, respectively, and y_i and y_j are the molar fraction of components i and j in the permeate stream, respectively.

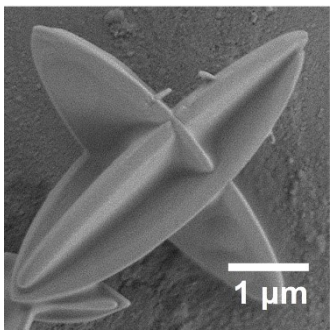

Figure S1. SEM image of pristine ZIF-L crystal.

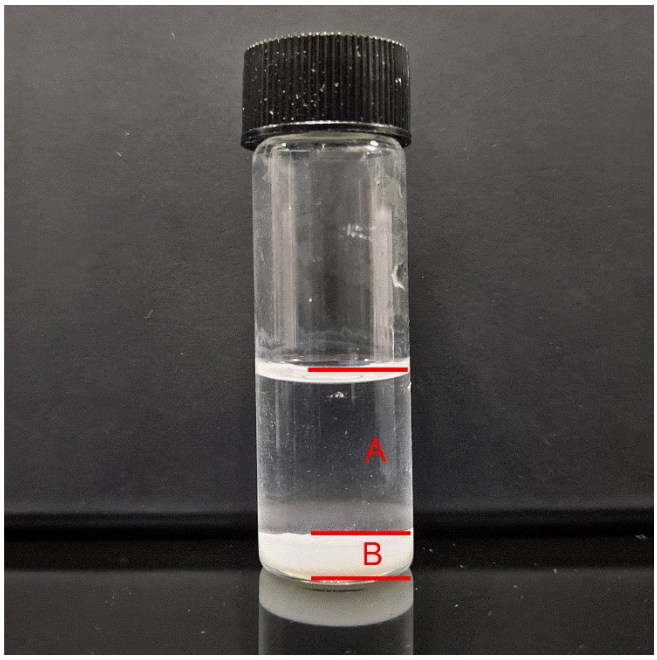

Figure S2. Transparent (A), and precipitated (B) part of RTD membrane precursor solution (Zn^{2+} + 2mIm in DMAc/H_2O solution)

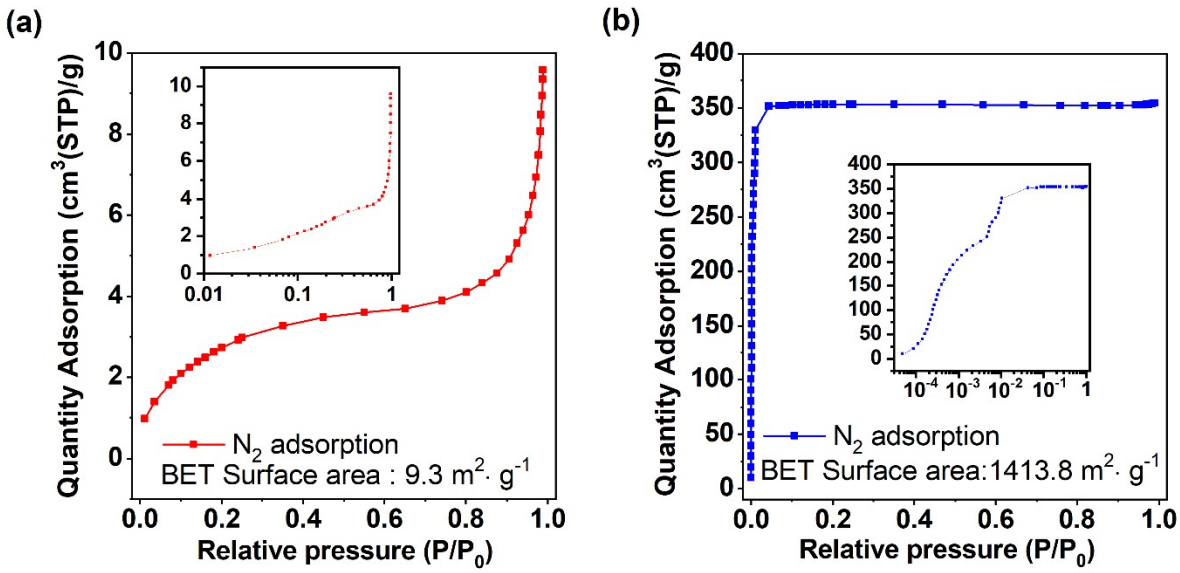

Figure S3. N_2 adsorption isotherm and corresponding BET surface area of (a) pristine ZIF-L crystals, and (b) hollow cross-leaf ZIF-8 crystals. Insert graph represent logarithmic-scale plot of each isotherm.

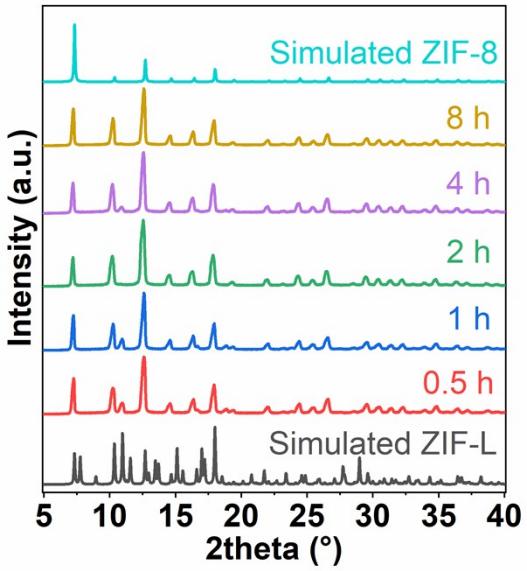

Figure S4. XRD patterns of ZIF-L crystals as a function of exposure time (0.5, 1, 2, 4, and 8 h) in RTD precursor solution ($Zn2^{+}$ + 2mIm in DMAc/H_2O) at 313 K.

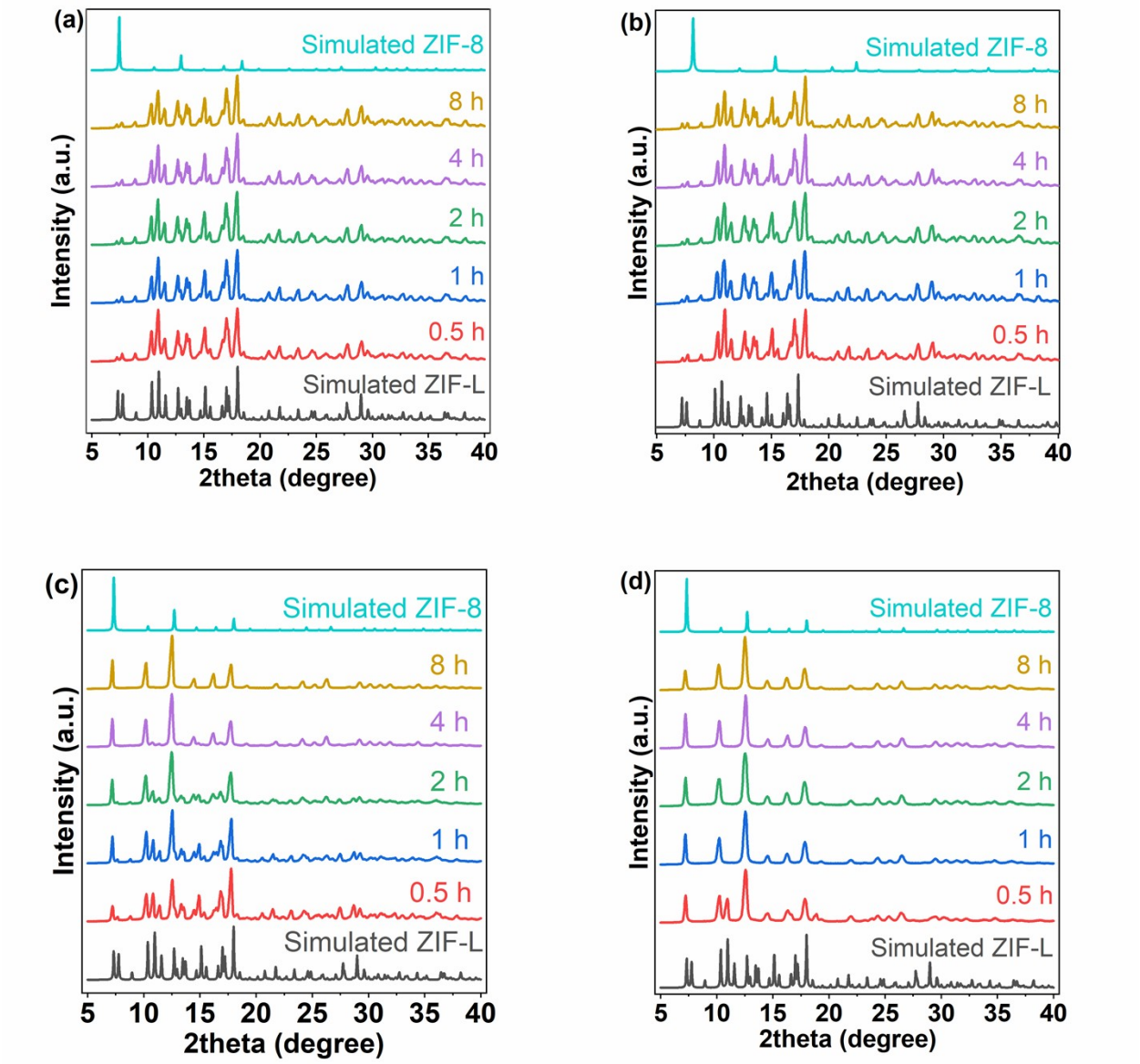

Figure S5. XRD patterns of ZIF-L crystals as a function of exposure time (0.5, 1, 2, 4, and 8 h) in only pure solvent (DMAc/H_2O = 2:1 v/v) in the absence of metal and ligand at (a) RT, (b) 313 K, (c) 333K, and (d) 353 K.

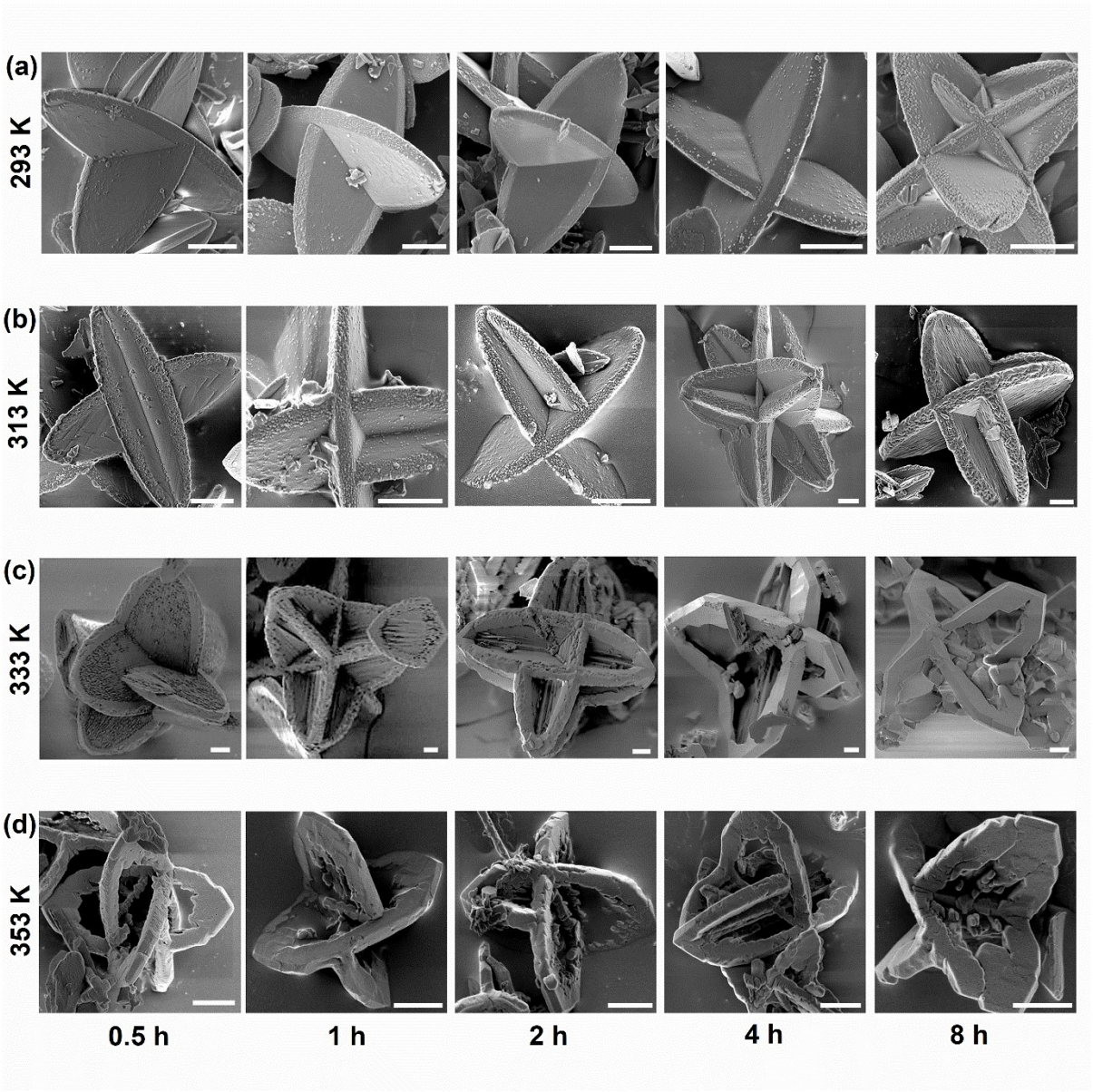

Figure S6. SEM images of ZIF-L crystals as a function of exposure time (0.5, 1, 2, 4, and 8 h) in only pure solvent (DMAc/H_2O = 2:1 v/v) in the absence of metal and ligand at (a) RT, (b) 313 K, (c) 333K, and (d) 353 K, Scale bars, 1μm.

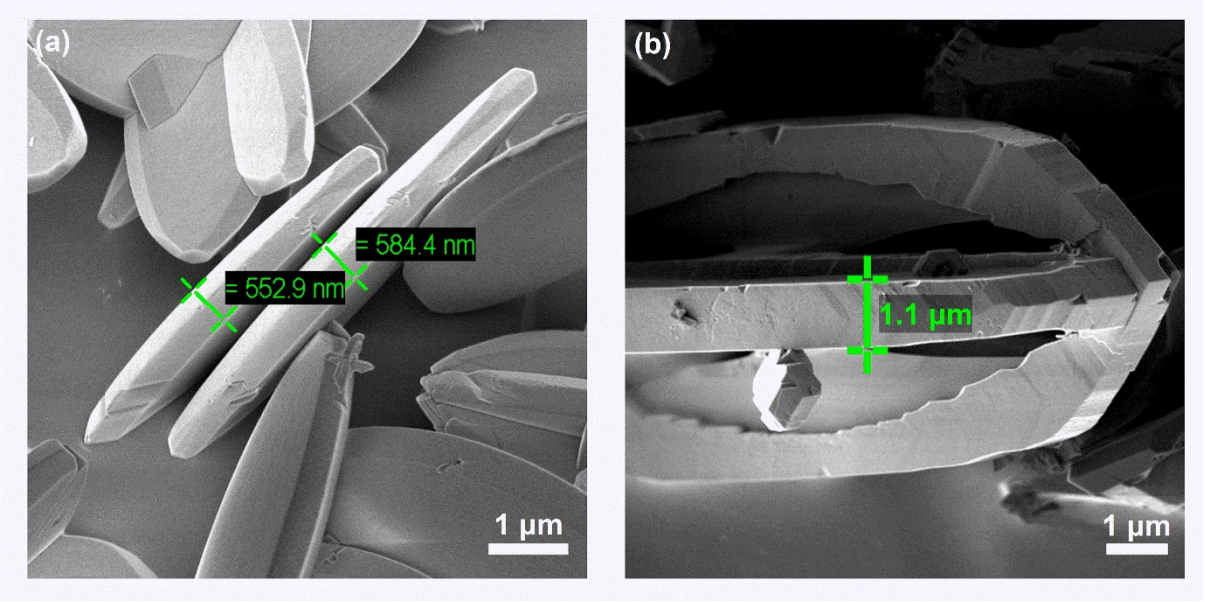

Figure S7. SEM images of (a) pristine ZIF-L and (b) hollow cross-leaf ZIF-8 crystal upon 8 h of DMAc/H_2O solvothermal treatment.

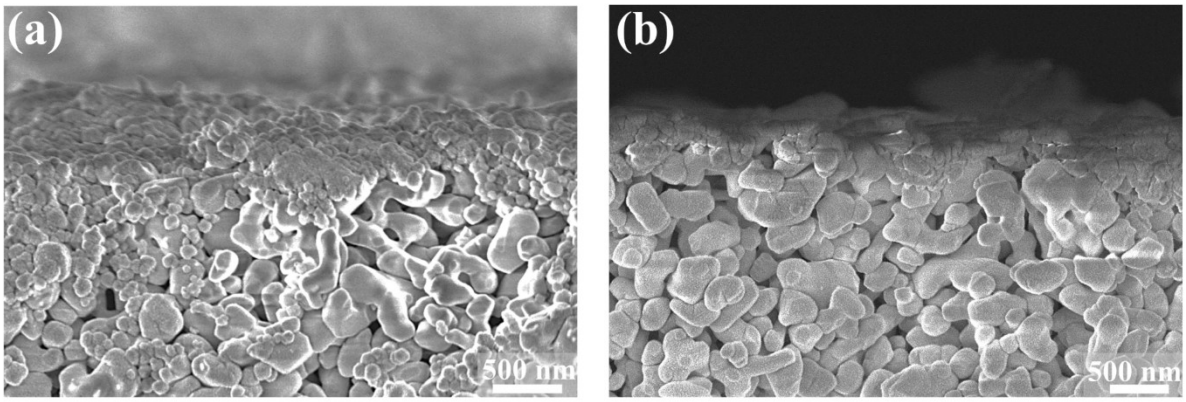

Figure S8. Cross-sectional SEM images of (a) Case 2 ZIF-8, and (b) Case 3 ZIF-L seed layer.

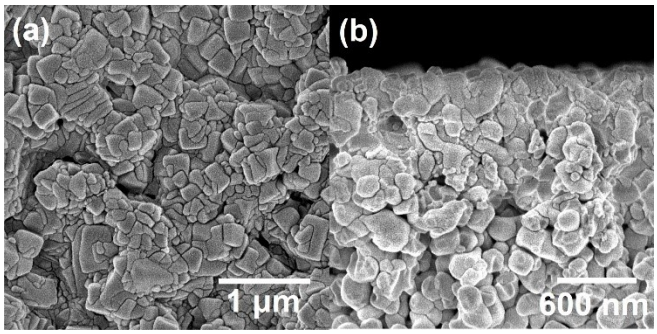

Figure S9. (a) Top view SEM image of defective Case 3 ZIF-8 membrane. Surface cracks were intentionally introduced via rapid drying of the membrane, (b) cross-sectional SEM image of defective Case 3 ZIF-8 membrane confirms no microstructural changes in the infiltrated layer.

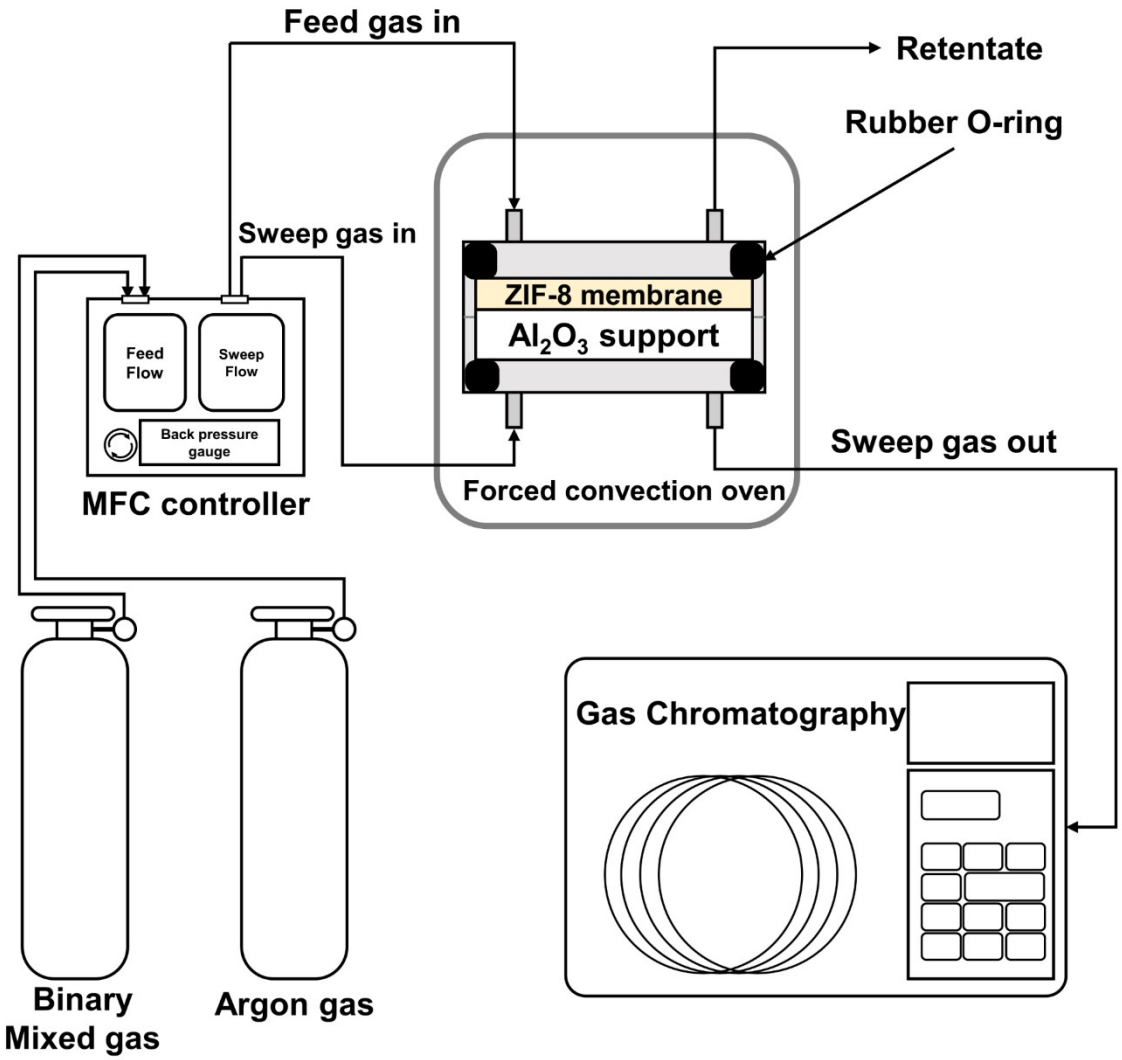

Figure S10. Schematic illustration of the experimental setup for the propylene/propane binary mixture permeation setup.

Table S1. Estimated each ZIF-8 layer (surface, and infiltrated) thickness of Case 1-3 membrane.

Index	Thickness (μm)		
	Case 1	**Case 2**	**Case 3**
Surface ZIF-8 layer	1.6 ± 0.3	1.2 ± 0.2	0.067 ± 0.08
Infiltrated ZIF-8 layer	2.9 ± 0.5	0.9 ± 0.1	0.49 ± 0.04

*Each value is measured from at least ten cross sections obtained at different locations of an individual sample and averaged with ten independently fabricated samples.

Table S2. Numerical permeance and selectivity values of Case 1-3 membranes. For each case, three independently prepared samples (M1-M3) were tested via steady-state Wicke-Kallenbach techniques at 293K.

Sample	Permeance (GPU)		Selectivity
	C_3H_6	C_3H_8	
Case 1 (M1)	31.6	1.2	25.8
Case 1 (M2)	30.9	1.5	20.7
Case 1 (M3)	33.9	1.5	23.2
Case 1 Average	**32.1±1.3**	**1.4±0.1**	**23.2±2.1**
Case 2 (M1)	159.2	3.9	41.0
Case 2 (M2)	154.7	4.2	36.5
Case 2 (M3)	161.4	3.1	52.0
Case 2 Average	**158.4±2.8**	**3.7±0.47**	**43.1±6.5**
Case 3 (M1)	381.3	8.8	43.4
Case 3 (M2)	389.6	7.7	50.6
Case 3 (M3)	386.2	7.1	54.4
Case 3 Average	**385.7±3.4**	**7.9±0.7**	**49.4±4.6**

Table S3. Representative literature summary of ZIF-8 membrane performances for propylene/propane separation.

Membrane type	Membrane Material	Support type	C_3H_6 permeance (GPU)	C_3H_6/C_3H_8 selectivity	Reference
Polymeric	Polyimide	Hollow fiber	0.2	12.2	4
			0.2	10	
			0.2	11.9	
			0.1	7.3	
	PPO	Film	0.1	4.3	5
	Ethylcellulose	Film	1.3	3.3	6
	Cellulose acetate		0.4	2.6	
	Polysulfone		1.6	1.4	
	PIM	Film	57.2	2.8	7
	PIM-CD-1 wt%		86.3	2.5	
	PIM-CD-2 wt%		100.6	2.4	
	PIM-1	Film	31.5	7.7	8
	6FDA-mPD	Film	0.01	10.0	9
	6FDA-IPDA		0.06	15.0	
	6FDA-6FpDA		0.09	16.0	
	6FDA-TeMPD	Film	1.9	8.6	10
	6FDA-TrMPD		1.5	11.0	
	6FDA-DDBT		0.04	27.0	
	6FDA-ODA		0.02	11.0	
	BPDA-TeMPD		0.2	13.0	
	PPO		0.1	9.1	
	P4MP		2.7	2.0	
	1.2PB		13.2	1.7	
	PDMS		334.3	1.1	
	PDMS/Silica-5%	Film	47.8	4.0	11
	PDMS/Silica-10%		38.5	4.5	
	PDMS/Silica-15%		31.7	5.2	
	PDMS/Silica-20%		15	6.8	
	PDMS/Silica-25%		9.7	7.3	
	PDMS/Silica-30%		4.3	10.2	
Carbon	Carbon derived PI	Film	5.8	10.0	12
	Carbon derived PI-LPSQ10	Hollow fiber	3.4	22.0	
	Carbon derived PI-LPSQ20		0.8	52.0	
	Carbon	Film	29.9	31.0	13
	Carbon derived from PAEK/Azide (50:50)-450ºC	Film	0.03	31.0	14
	Carbon derived from PAEK/Azide (80:20)-450ºC		0.1	17.0	
	Carbon derived from PAEK/Azide (50:50)-550ºC		0.02	48.0	
	Carbon derived from PAEK/Azide (80:20)-550ºC		0.9	44.0	

	Carbon derived from PAEK/Azide (50:50)-650ºC		0.01	24.0	
	Carbon derived from PAEK/Azide (80:20)-650ºC		0.01	16.0	
	Carbon derived from 6FDA-based polyimide polymer	γ-Al_2O_3 disk	9.6	36.0	[15]
	Carbon derived from BPDA-DDBT/DABA asymmetric (600°C)	Hollow fiber	20.0	14.0	[16]
	Carbon derived from BPDA-DDBT/DABA asymmetric (625°C)		34.0	17.0	
ZIFs	ZIF-8	α-Al_2O_3 disk	85.1	34.0	[17]
			82.7	35.0	
			73.2	31.0	
			61.5	45.0	
			113.0	28.0	
	ZIF-8	α-Al_2O_3 disk	23.3	89.0	[18]
			24.8	63.0	
			46.6	50.0	
			32.9	75.0	
			49.9	44.0	
	ZIF-8	α-Al_2O_3 disk	19.1	51.0	[19]
			16.4	50.0	
			23.0	47.0	
			20.9	53.0	
			17.6	51.0	
			18.5	61.0	
	ZIF-8	α-Al_2O_3 disk	32.9	30.0	[20]
			26.7	28.9	
			22.8	28.1	
			18.1	26.9	
	ZIF-8	α-Al_2O_3 Hollow fiber	7.5	59.0	[21]
	ZIF-8	α-Al_2O_3 disk	35.8	20.0	[22]
			15.5	7.2	
			116.5	6.9	
	ZIF-8		253.7	36.0	[23]
	ZIF-67	α-Al_2O_3 disk	137.7	84.8	[24]
	ZIF-8/ ZIF-67		110.5	209.1	
	ZIF-67/ ZIF-67		92.3	163.2	
	ZIF-8	α-Al_2O_3 disk	63.6	50.0	[25]
	ZIF-8	α-Al_2O_3 disk	37.3	120.0	[26]
	ZIF-8	α-Al_2O_3 disk	62.1	40.4	[27]
			43	30.8	

	ZIF-8	α-Al_2O_3 disk	80.3	70.6	[28]
			160.7	22.4	
			118.0	28.0	
			80.0	38.0	
			92.0	33.1	
			58.2	39.7	
	ZIF-8	α-Al_2O_3 disk	233.0	40.0	[29]
	ZIF-8	Hollow fiber	45.1	184.4	[30]
			33.4	176.2	
			29.5	135.0	
			27.3	90.3	
	ZIF-8	Hollow fiber	66.0	65.0	[31]
			34.0	24.0	
	ZIF-8	α-Al_2O_3 disk	10.2	26.0	[32]
	MFI ZIF-8		21.4	32.0	
	MFI nanosheet ZIF-8		46.5	33.0	
	MFI + MFI nanosheet ZIF-8		66.4	72.0	
	ZIF-8	Hollow fiber	26.9	12.0	[33]
	ZIF-8	α-Al_2O_3 disk supported by γ-Al_2O_3	113.8	104.0	[34]
			63.9	141.0	
			110	152.0	
			134	45.0	
			136.2	67.0	
			253.58	72.0	
			185.5	46.0	
			262.8	71.0	
			479.7	74.0	
	Case 1	α-Al_2O_3 disk	32.1	23.2	This report
	Case 2		158.4	43.1	
	Case 3		385.7	49.4	

References

1 Y. Pan, Y. Liu, G. Zeng, L. Zhao and Z. Lai, *Chem. Commun.*, 2011, **47**, 2071–2073.

2 K. Eum, M. Hayashi, M. D. De Mello, F. Xue, H. T. Kwon and M. Tsapatsis, *Angew. Chemie*, 2019, **131**, 16542–16546.

3 M. N. Shah, M. A. Gonzalez, M. C. McCarthy and H. K. Jeong, *Langmuir*, 2013, **29**, 7896–7902.

4 J. J. Krol, M. Boerrigter and G. H. Koops, *J. Memb. Sci.*, 2001, **184**, 275–286.

5 S. Bai, S. Sridhar and A. A. Khan, *J. Memb. Sci.*, 1998, **147**, 131–139.

6 S. Sridhar and A. A. Khan, *J. Memb. Sci.*, 1999, **159**, 209–219.

7 J. Liu, Y. Xiao and T. S. Chung, *J. Mater. Chem. A*, 2017, **5**, 4583–4595.

8 P. Li, T. S. Chung and D. R. Paul, *J. Memb. Sci.*, 2013, **432**, 50–57.

9 C. Staudt-Bickel and W. J. Koros, *J. Memb. Sci.*, 2000, **170**, 205–214.

10 K. Okamoto, K. Noborio, J. Hao, K. Tanaka and H. Kita, *J. Memb. Sci.*, 1997, **134**, 171–179.

11 H. Kim, H. G. Kim, S. Kim and S. S. Kim, *J. Memb. Sci.*, 2009, **344**, 211–218.

12 J. H. Shin, H. J. Yu, J. Park, A. S. Lee, S. S. Hwang, S. J. Kim, S. Park, K. Y. Cho, W. Won and J. S. Lee, *J. Memb. Sci.*, 2020, **598**, 117660.

13 Z. Qiao, Z. Wang, C. Zhang, S. Yuan, Y. Zhu and J. Wang, *AIChE J.*, 2012, **59**, 215–228.

14 M. L. Chng, Y. Xiao, T. S. Chung, M. Toriida and S. Tamai, *Carbon N. Y.*, 2009, **47**, 1857–1866.

15 X. Ma, B. K. Lin, X. Wei, J. Kniep and Y. S. Lin, *Ind. Eng. Chem. Res.*, 2013, **52**, 4297–4305.

16 K. ichi Okamoto, S. Kawamura, M. Yoshino, H. Kita, Y. Hirayama, N. Tanihara and Y. Kusuki, *Ind. Eng. Chem. Res.*, 1999, **38**, 4424–4432.

17 Y. Pan, T. Li, G. Lestari and Z. Lai, *J. Memb. Sci.*, 2012, **390**–**391**, 93–98.

18 Y. Pan, W. Liu, Y. Zhao, C. Wang and Z. Lai, *J. Memb. Sci.*, 2015, **493**, 88–96.

19 J. Yu, Y. Pan, C. Wang and Z. Lai, *Chem. Eng. Sci.*, 2016, **141**, 119–124.

20 D. Liu, X. Ma, H. Xi and Y. S. Lin, *J. Memb. Sci.*, 2014, **451**, 85–93.

21 N. Hara, M. Yoshimune, H. Negishi, K. Haraya, S. Hara and T. Yamaguchi, *J. Memb. Sci.*, 2014, **450**, 215–223.

22 N. Hara, M. Yoshimune, H. Negishi, K. Haraya, S. Hara and T. Yamaguchi, *Microporous Mesoporous Mater.*, 2015, **206**, 75–80.

23 S. Tanaka, K. Okubo, K. Kida, M. Sugita and T. Takewaki, *J. Memb. Sci.*, 2017, **544**, 306–311.

24 H. T. Kwon, H. K. Jeong, A. S. Lee, H. S. An and J. S. Lee, *J. Am. Chem. Soc.*, 2015, **137**, 12304–12311.

25 H. T. Kwon and H. K. Jeong, *J. Am. Chem. Soc.*, 2013, **135**, 10763–10768.

26 H. T. Kwon, H. K. Jeong, A. S. Lee, H. S. An, T. Lee, E. Jang, J. S. Lee and J. Choi, *Chem. Commun.*, 2016, **52**, 11669–11672.

27 H. T. Kwon and H. K. Jeong, *Chem. Commun.*, 2013, **49**, 3854–3856.

28 H. T. Kwon and H. K. Jeong, *Chem. Eng. Sci.*, 2015, **124**, 20–26.

29 M. J. Lee, H. T. Kwon and H. K. Jeong, *Angew. Chemie - Int. Ed.*, 2018, **57**, 156–161.

30 K. Eum, C. Ma, A. Rownaghi, C. W. Jones and S. Nair, *ACS Appl. Mater. Interfaces*, 2016, **8**, 25337–25342.

31 K. Eum, A. Rownaghi, D. Choi, R. R. Bhave, C. W. Jones and S. Nair, *Adv. Funct. Mater.*, 2016, **26**, 5011–5018.

32 K. Eum, S. Yang, B. Min, C. Ma, J. H. Drese, Y. Tamhankar and S. Nair, *ACS Appl. Mater. Interfaces*, 2020, **12**, 27368–27377.

33 A. J. Brown, N. A. Brunelli, K. Eum, F. Rashidi, J. R. Johnson, W. J. Koros, C. W. Jones and S. Nair, *Science.*, 2014, **345**, 72–75.

34 X. Ma, P. Kumar, N. Mittal, A. Khlyustova, P. Daoutidis, K. Andre Mkhoyan and M. Tsapatsis, *Science.*, 2018, **361**, 1008–1011.